HHS Public Access

Author manuscript

Nat Med. Author manuscript; available in PMC 2017 November 15.

Published in final edited form as:

Nat Med. 2017 June ; 23(6): 714–722. doi:10.1038/nm.4340.

CX_3CR1^+ monocytes modulate learning and learning-dependent dendritic spine remodeling via TNFα

Juan Mauricio Garré[1], **Hernandez Moura Silva**[2], **Juan J. Lafaille**[2], and **Guang Yang**[1]

[1]Department of Anesthesiology, Perioperative Care and Pain Medicine, New York University School of Medicine, New York, NY, 10016, USA

[2]Skirball Institute of Biomolecular Medicine, Molecular Pathogenesis. Departments of Pathology and Medicine, New York University School of Medicine, New York, NY, 10016, USA

Abstract

Impaired learning and cognitive function often occurs during systemic infection or inflammation. Although activation of the innate immune system has been linked to the behavioral and cognitive effects that are associated with infection, the underlying mechanisms remain poorly understood. Here we mimicked viral immune activation with poly(I:C), a synthetic analog of double-stranded RNA, and longitudinally imaged postsynaptic dendritic spines of layer V pyramidal neurons in the mouse primary motor cortex using two-photon microscopy. We found that peripheral immune activation caused dendritic spine loss, impairments in learning-dependent dendritic spine formation and deficits in multiple learning tasks in mice. These observed synaptic alterations in the cortex were mediated by peripheral-monocyte-derived cells and did not require microglial function in the central nervous system. Furthermore, activation of $CX_3CR1^{high}Ly6C^{low}$ monocytes impaired motor learning and learning-related dendritic spine plasticity through tumor necrosis factor (TNF)-α-dependent mechanisms. Taken together, our results highlight CX_3CR1^{high} monocytes and TNF-α as potential therapeutic targets for preventing infection-induced cognitive dysfunction.

Activation of the immune system has profound effects on the function of the central nervous system (CNS)[1, 2, 3, 4, 5], and it is thought to have an important role in schizophrenia[6], autism-spectrum disorder[7] and the neuropsychological impairment associated with infectious diseases[8]. Indeed, changes in mood and cognitive function are frequently observed in people who are infected with viruses, such as influenza and HIV, or

Correspondence should be addressed to G.Y. (Guang.Yang@med.nyu.edu).

AUTHOR CONTRIBUTIONS

J.M.G., H.M.S., J.J.L., and G.Y. designed the experiments. J.M.G. performed the in vivo imaging experiments, animal behavior assays and biochemical experiments. J.M.G. and H.M.S. performed the flow cytometry experiments. All of authors contributed to data analysis and interpretation. J.M.G. and G.Y. wrote the manuscript.

COMPETING FINANCIAL INTERESTS

The authors declare no competing financial interests.

Data availability.

All data used in this study are available upon request.

bacteria[9, 10, 11, 12, 13]. The similarity of behavioral effects that are associated with different infectious diseases suggests that immune responses to infectious agents, rather than a specific pathogen per se, may have a critical role in cognitive decline. Administration of polyinosinic-polycytidylic acid (poly(I:C)) is a widely used model to study virus-associated immune activation[14]. Double-stranded RNA is produced during viral replication[15] and recognized by the mammalian innate immune system primarily through pathogen recognition receptors (PRRs), such as toll-like receptor 3 (TLR3)[16]. The binding of poly(I:C) to PRRs leads to the expression of a series of immune mediators (such as type 1 interferons (IFNs), pro-inflammatory cytokines and chemokines), a process that efficiently mimics the acute phase of viral infection[17]. Similar to that observed in viral infection, peripheral immune stimulation through poly(I:C) has been shown to cause behavioral and cognitive impairments in both developing and adult animals[18, 19, 20, 21]; however, the underlying mechanisms remain unclear.

Various host immune cells are involved in innate defense against infection. Monocytes are a population of leukocytes that are derived from progenitors in the bone marrow and that circulate in the bloodstream[22]. They develop into macrophages or dendritic cells after entering peripheral tissues. In response to infection, monocytes take part in the inflammatory response by producing and releasing pro-inflammatory cytokines, such as TNF-α, and chemokines in the infected areas[23, 24, 25]. In the CNS, microglia are the major innate immune cells that become activated during systemic infection[26]. Like monocytes, activated microglia produce a number of inflammatory molecules and have been implicated in the development of neurodegenerative diseases[5]. Despite the fact that monocytes and microglia are crucial players in innate immunity, which of these populations is involved in the alteration of CNS functions during virus-associated immune activation remains unknown. It is also unclear how activation of these cells alters neuronal circuits and leads to learning and behavioral deficits. Here we show that peripheral immune activation causes deficits in learning tasks, synapse loss and a reduction in learning-dependent synapse formation. These synaptic and behavioral changes are mediated by CX_3CR1^{high} monocytes via TNF-α-dependent mechanisms.

RESULTS

Systemic immune challenge increases dendritic spine dynamics in the cortex

To investigate how peripheral immune activation affects the brain, we intraperitoneally (i.p.) administered poly(I:C) to adolescent (postnatal day (P) 30) transgenic mice that expressed yellow fluorescent protein in layer V (L5) pyramidal neurons (Thy1-YFP mice) and examined structural changes in the postsynaptic dendritic spines of the primary motor cortex using transcranial two-photon microscopy (Fig. 1a)[27]. After a single injection with either 5 or 50 mg per kg body weight (mg/kg) poly(I:C), we observed more dendritic spine remodeling over 2 d in poly(I:C)-treated mice than in vehicle-treated control mice (Fig. 1a,b). In control mice, 8.3 ± 0.6% of dendritic spines were eliminated and 7.2 ± 0.7% were formed, whereas in mice that were treated with 5 mg/kg poly(I:C), 17.5 ± 1.1% and 14.0 ± 0.9% of dendritic spines were eliminated and formed, respectively. A significant increase in spine elimination and formation was also detected 24 h after poly(I:C) injection (Fig. 1c

and Supplementary Table 1). The rate of spine elimination after poly(I:C) injection was higher than that of spine formation (Supplementary Fig. 1), indicating a net loss of spines over 1–2 d (Fig. 1d). Four days after poly(I:C) injection, no continued increase in spine remodeling was detected relative to that in control mice (Fig. 1b), indicating an acute effect of poly(I:C) treatment on spine dynamics. Consistent with previous reports[28, 29], we found that dendritic spine remodeling was lower in 2-month-old mice than in 1-month-old mice. However, similar to what was observed in 1-month-old mice, poly(I:C) injection (5 mg/kg) at P60 significantly increased the rates of spine elimination and formation over 2 d (Fig. 1e,f).

Systemic immune challenge impairs dendritic spine plasticity associated with learning

The remodeling of synaptic connections is important for learning and memory formation[29, 30, 31, 32, 33]. Previous studies have shown that the learning of motor skills causes a learning-dependent increase in dendritic spine formation in the motor cortex and that the extent of new spine formation correlates with an improvement in the animal's performance after learning[29, 32]. We next investigated whether poly(I:C) injection similarly altered learning-dependent spine remodeling. We trained 1- or 2-month-old mice to run on an accelerating rotating rod (which is referred to as a rotarod) and imaged the same dendrites in the motor cortex before and after a 2-d period of training (Fig. 2a). Two days after rotarod training, we observed a significant reduction in learning-dependent spine formation in poly(I:C)-treated mice as compared to that in the age-matched controls (Fig. 2b,c and Supplementary Table 1). Conversely, we found a significant increase in spine elimination in poly(I:C)-treated mice as compared to that of vehicle-treated controls. Thus, in poly(I:C)-treated mice the combined result of these modifications is a net loss of spines after learning, while vehicle-treated mice exhibit a net gain in spines after learning (Fig. 2d,e). Furthermore, although poly(I:C) treatment had no effects on the initial performance of the mice in the rotarod task (Fig. 2f,g) or on their body weight (Supplementary Fig. 2) as compared to those observed in vehicle-treated mice, poly(I:C) treatment did cause a significant reduction in motor performance improvements after a 2-d training period in both 1- and 2-month-old mice (Fig. 2h,i).

To evaluate the long-term effect of poly(I:C) treatment on learning-related spine remodeling and motor performance, we reimaged and tested 2-month-old mice on P67, after a 5-d period without further rotarod training (Fig. 2a). We found that of the new spines formed during the 2-d training interval (from P60 to P62), fewer persisted at P67 in the poly(I:C)-treated mice than in the control mice (Fig. 2j). Furthermore, motor performance improvement continued to remain lower in the poly(I:C)-treated mice (Fig. 2k). There was a significant correlation between the percentage of training-related persistent new spines and rotarod performance on P67 (Fig. 2l). We also compared the performance of poly(I:C)- and vehicle-treated mice in a 'novel object recognition' (NOR) test (Supplementary Fig. 3). NOR training was performed 24 h after poly(I:C) administration. The training and test sessions were separated by either a 1-h or a 24-h interval to examine the short-term and long-term memory, respectively, of the mice. Although vehicle-treated control mice showed a preference for the novel object during the NOR test, mice that were pretreated with

poly(I:C) showed no such preference at either 1 h or 24 h after training, indicating impaired recognition memory.

CX_3CR1^+ cells are crucial for poly(I:C)-induced dendritic spine instability

The chemokine receptor CX_3CR1 is widely expressed in monocytes and monocyte-derived cells in peripheral tissues, and it is exclusively expressed in microglia in the CNS parenchyma[34]. To determine whether the observed effects of poly(I:C) treatment on dendritic spine plasticity require the involvement of CX_3CR1^+ cells, we performed *in vivo* diphtheria toxin receptor (DTR)-mediated cell depletion. Specifically, *Cx3cr1*^{CreER} mice, which express a tamoxifen-inducible Cre recombinase (CreER) under the control of the endogenous *Cx3cr1* promoter, were crossed with mice harboring the ubiquitous *Rosa26-stop-DTR* (*R26*^{iDTR}) allele, permits DTR expression where Cre is present. For *in vivo* cell depletion, *Cx3cr1*$^{CreER/+}$;*R26*$^{iDTR/+}$ mice were given tamoxifen for 3 d (P54 to 56) and subsequently treated with diphtheria toxin (DT) for 3 d (P57 to 59) (Fig. 3a). We found that the majority of CX_3CR1^+ cells, including peripheral $CD11b^+$ cells and CNS microglia, were depleted after the last DT treatment (Fig. 3b–d). One day after the last DT treatment, we administered poly(I:C) and examined the rates of spine remodeling in the cortex over the next 2 d. Similarly to that seen in wild-type (WT) mice, we found a significant increase in spine elimination and formation in control mice that were not depleted for CX_3CR1^+ cells (*Cx3cr1*$^{CreER/+}$) at 2 d after the administration of poly(I:C) (Fig. 3e). In contrast, in mice that were depleted of CX_3CR1^+ cells (*Cx3cr1*$^{CreER/+}$;*R26*$^{iDTR/+}$), poly(I:C) treatment had no significant effects on the rates of dendritic spine elimination and formation (Fig. 3f), indicating the requirement of CX_3CR1^+ cells in dendritic spine remodeling in the cortex.

Although CX_3CR1 is mostly expressed in cells of the myeloid lineage, a small fraction of T cells (which are cells of the lymphoid lineage) may also express CX_3CR1 (ref. 34). To determine whether T cells were involved in poly(I:C)-induced spine remodeling, we examined dendritic spine plasticity in *Rag1*$^{-/-}$ mice, which are deficient for T cells and B cells. We found that administration of poly(I:C) significantly increased the rates of spine elimination and formation in *Rag1*$^{-/-}$ mice, relative to those observed after treatment with vehicle only, and that these were comparable to the rates observed in WT mice (Fig. 3g), suggesting the role of CX_3CR1^+ myeloid cells but not of CX_3CR1^+ T cells in poly(I:C)-induced synapse alteration.

CNS microglia are not required for poly(I:C)-induced dendritic spine instability

Previous studies have shown that microglia are important for synapse formation and elimination under both physiological and pathological conditions[35, 36, 37]. To determine which population of CX_3CR1^+ cells (central or peripheral) regulates cortical spine plasticity during peripheral immune activation, we restricted cell depletion to that of CNS microglia by taking advantage of a previously established strategy in which *Cx3cr1*$^{CreER/+}$ mice that are used ~30 d after tamoxifen administration permit Cre-dependent manipulation of gene expression almost exclusively in CNS-resident macrophages, including microglia[35, 38]. This strategy is based on the fact that yolk-sac-derived microglia are a self-renewing population with low turnover rates (months to years)[39, 40, 41], whereas most peripheral circulating CX_3CR1^+ populations have a high turnover rate (<1 week) and are rapidly replenished

through bone marrow (BM) precursors[42, 43]. Consistent with previous studies[35], when we gave *Cx3cr1*$^{CreER/+}$;*R26*$^{iDTR/+}$ mice tamoxifen at P30 to P32, and then administered DT ~1 month later (P57 to P59) (Fig. 4a), we found that CNS microglia were largely depleted, whereas the CX_3CR1^+ population in blood was mostly intact, after the last DT treatment (Fig. 4b and Supplementary Fig. 4). Moreover, there was no significant difference in levels of the inflammatory cytokine TNF-α in blood and brain (cortex) between control and microglia-depleted mice (Supplementary Fig. 4). Notably, when mice depleted of microglia were challenged with poly(I:C), we found a significant increase in dendritic spine elimination and formation in the cortex after 2 d (Fig. 4c). The increase in spine turnover after poly(I:C) treatment was comparable to that observed in nondepleted control mice with intact CNS microglia, indicating that systemic immune challenge alters spine dynamics in the cortex in the absence of microglia. Consistent with this finding, we found no morphological signs of microglial activation in the motor cortex at 24 h after poly(I:C) administration (Supplementary Fig. 5).

CX_3CR1^+ monocytes mediate poly(I:C)-induced synaptic and learning deficits

To further establish the function of peripheral CX_3CR1^+ monocytes on dendritic spine remodeling during systemic immune challenge, we transplanted BM cells obtained from *Cx3cr1*$^{CreER/+}$;*R26*$^{iDTR/+}$ mice into irradiated WT recipients (referred to as *Cx3cr1*$^{CreER/+}$;*R26*$^{iDTR/+}$→WT chimeras) to generate chimeric mice that express *Cx3cr1*$^{CreER/+}$;*R26*$^{iDTR/+}$ only in peripheral tissues. One month after BM reconstitution, mice were given tamoxifen and subsequently treated with DT (Fig. 4d). Flow cytometry analysis revealed a substantial reduction in the number of $CX_3CR1^+CD11b^+$ cells in the blood and liver tissues of the *Cx3cr1*$^{CreER/+}$;*R26*$^{iDTR/+}$→WT chimeras as compared to that in their control counterparts that received BM cells from *Cx3cr1*$^{CreER/+}$ mice (*Cx3cr1*$^{CreER/+}$→WT chimeras), indicating a reduction of CX_3CR1^+ monocytes and monocyte-derived cells. In contrast, DT treatment had no effect on the number of CNS microglia in the cortex of the *Cx3cr1*$^{CreER/+}$;*R26*$^{iDTR/+}$→WT chimeras (Fig. 4e and Supplementary Fig. 6).

Next we examined the effect of poly(I:C) treatment on the baseline and learning-induced remodeling of dendritic spines in the motor cortex. Poly(I:C) treatment significantly increased the baseline spine elimination and formation rates in nondepleted control mice (Fig. 4f), whereas poly(I:C) treatment had no significant effects on the baseline rates of spine turnover in mice that were depleted of CX_3CR1^+ monocytes (Fig. 4g). Furthermore, in contrast to control mice, which showed impaired learning-dependent spine remodeling and a reduction in the total number of spines, poly(I:C) treatment caused no changes in motor-learning-dependent spine remodeling or in total spine number in chimeras in which CX_3CR1^+ monocytes were depleted (Fig. 4h–k and Supplementary Fig. 7). An improvement in performance after rotarod motor learning was also not impaired in these mice after poly(I:C) administration (Fig. 4l–o). Taken together, these results indicate that the effect of systemic immune challenge on learning and learning-dependent dendritic spine remodeling is mainly mediated by peripheral CX_3CR1^+ monocytes.

To further investigate the role of monocytes in poly(I:C)-induced dendritic spine alteration, we collected leukocytes from blood and spleen tissues and magnetically sorted them on the basis of the cell surface expression of CD11b, a marker for myeloid cells (including monocytes). Mice that were depleted of CX_3CR1^+ cells (in both the CNS and periphery) were injected with various amounts of CD11b-sorted cells. We found that poly(I:C) treatment significantly increased spine elimination and formation in mice that were injected with 2×10^6 CD11b-sorted cells, as compared to that in vehicle-treated mice (Supplementary Fig. 8). The rates of spine elimination and formation after poly(I:C) administration were significantly lower in mice that were adoptively transferred with a lower number (0.5×10^6) of CD11b-sorted cells than in those that were adoptively transferred with 2×10^6 CD11b-sorted cells. We did not find changes in spine turnover in mice that were injected with the fraction of cells that did not express CD11b.

CX_3CR1^{high} monocytes are required for poly(I:C)-induced synaptic and learning deficits

Previous work has identified that two distinct subsets of peripheral blood monocytes exist in mice, based on the level of CX_3CR1 expression (CX_3CR1^{low} and CX_3CR1^{high})[44]. When we examined the expression of Ly6C, a marker for inflammatory monocytes, in CX_3CR1^+ cells, we found that systemic or peripheral depletion of CX_3CR1^+ cells substantially reduced the number of $CX_3CR1^{high}Ly6C^{low}$ monocytes in the blood, whereas $CX_3CR1^{low}Ly6C^{high}$ monocytes were not affected (Supplementary Fig. 9). These results suggest that $CX_3CR1^{high}Ly6C^{low}$ monocytes, a population of monocytes that patrol blood vessels[24], are essential for poly(I:C)-induced cortical changes.

To test the role of CX_3CR1^{high} monocytes in poly(I:C)-induced synaptic deficits, we took advantage of the fact that CX_3CR1 deficiency leads to a substantial reduction of CX_3CR1^{high} monocytes[45], and generated *Cx3cr1*$^{-/-}$→WT chimeric mice, which have a deficiency of CX_3CR1 in peripheral leukocytes (Fig. 5a). In *Cx3cr1*$^{-/-}$→WT mice, we found that poly(I:C) administration had no significant effects on the baseline rates of dendritic spine elimination and formation in the motor cortex (Fig. 5b,c). Moreover, motor learning-induced spine formation and elimination were not affected by the administration of poly(I:C) before the training (Fig. 5d,e). As a result, there were no changes in total spine number after poly(I:C) administration in *Cx3cr1*$^{-/-}$→WT mice (Fig. 5f,g). Furthermore, administration of poly(I:C) in *Cx3cr1*$^{-/-}$→WT chimeric mice had no significant effects on baseline performance in the rotarod test and on performance improvement after training, as compared to that observed after treatment with vehicle (Fig. 5h–k). Thus, systemic immune challenge impairs dendritic spine plasticity and learning through the involvement of CX_3CR1^{high} monocytes.

CX_3CR1^{high} monocytes contribute to increased TNF-α levels in the cortex

CX_3CR1 signaling in CX_3CR1^{high} monocytes has been linked to the production of TNF-α and chemokines[24]. To explore the molecular mechanisms that mediate the effects of CX_3CR1^{high} monocytes on dendritic spine plasticity, we measured the protein levels of pro-inflammatory cytokines at various time points after poly(I:C) injection. In WT mice, poly(I:C) treatment caused a transient increase in cytokine production in the peripheral circulation (Fig. 6a and Supplementary Fig. 10). Plasma levels of TNF-α, interleukin (IL)-6,

IL-1β and IFN-β were substantially increased at 3 h after poly(I:C) injection, relative to those in vehicle-injected mice (Fig. 6a and Supplementary Fig. 10). Notably, we found a significant increase in TNF-α levels in the cortex at 3–24 h after poly(I:C) injection (Fig. 6b and Supplementary Fig. 11), whereas there were no changes in IL-6 and IL-1β levels (Supplementary Fig. 10); the amount of IFN-β in the cortex was below that detectable by the ELISA.

To determine whether CX_3CR1^{high} monocytes are required for the poly(I:C)-induced increase in TNF-α levels in the cortex, we performed ELISA measurements in mice that were depleted of either CNS microglia or peripheral monocytes (Supplementary Fig. 12). We found that there were significantly more amounts of TNF-α in the cortex of mice that were depleted of microglia but that had an intact blood monocyte population at 24 h after poly(I:C) administration than in mice that were treated with vehicle. In contrast, in mice that were depleted of CX_3CR1^{+} monocytes but that had intact CNS microglia, poly(I:C) treatment had no significant effect on the TNF-α levels in the cortex, relative to the levels observed in the vehicle-treated controls. Together with the finding that mice depleted of CX_3CR1^{+} monocytes had reduced numbers of $CX_3CR1^{high}Ly6C^{low}$ blood monocytes (Supplementary Fig. 9), these results suggest that CX_3CR1^{high} monocytes are required for the increase in brain TNF-α levels during systemic immune challenge.

TNFα mediates poly(I:C)-induced synaptic and learning deficits

Previous studies have shown that TNF-α has an important role in synapse plasticity[46, 47, 48, 49]. Given our findings that CX_3CR1^{high} monocytes are required for poly(I:C)-induced spine remodeling and increased TNF-α levels in the cortex, we hypothesized that the effect of systemic immune challenge on learning and learning-dependent synapse plasticity are mediated by this monocyte subset through TNF-α signaling. In $Tnf^{-/-}$ mice (which do not produce TNF-α), we found that poly(I:C) administration had no significant effects on the rates of dendritic spine elimination and formation over 2 d, whereas intravenous administration of exogenous TNF-α significantly increased the rates of spine elimination and formation (Fig. 6c). Furthermore, administration of the dominant-negative form of TNF-α (hereafter referred to as DN-TNF), which binds to soluble TNF-α, abolished poly(I:C)-induced increase in baseline spine turnover in WT mice (Fig. 6d).

Several lines of evidence have suggested that systemic inflammation or increased amounts of TNF-α may change the permeability of the blood–brain barrier (BBB)[50]. To control for the potential effects of BBB disruption on spine remodeling, we administered poly(I:C) to mice that were treated with SB-3CT, which protects the BBB by inhibiting matrix metalloproteinase 9 (MMP9)[51] (Supplementary Fig. 13), and found that treatment with poly(I:C) substantially increased spine remodeling in SB-3CT-treated mice. Furthermore, there were no changes in the number of $CD45^{high}CD11b^{+}$ cells in the cortex 2 d after poly(I:C) administration (Supplementary Fig. 14). Taken together, these results suggest that the deleterious effects of poly (I:C) on spine remodeling are mediated by increased TNF-α production, rather than due to BBB disruption and subsequent entry of blood monocytes into the cortex.

To investigate whether diminishing TNF-α production by monocytes could protect the mice from synaptic and learning impairments, we generated *Tnf*$^{-/-}$→WT chimeras that were unable to produce TNF-α in leukocytes. One month after BM transplantation, we administered poly(I:C) to these mice and examined baseline spine turnover, motor-learning-dependent spine plasticity, as well as performance improvement after motor training (Fig. 6e). We found that poly(I:C) treatment had no significant effects on the rates of spine elimination and formation under both baseline (Fig. 6f) and motor-learning conditions (Fig. 6g,h and Supplementary Fig. 15) in *Tnf*$^{-/-}$→WT mice. Furthermore, mice that were deficient for TNF-α production by leukocytes did not show motor learning deficits after poly(I:C) administration (Fig. 6i,j). As a control, we administered poly(I:C) to *Il6*$^{-/-}$→WT chimeras, in which IL-6 production by leukocytes was abolished, and examined spine plasticity in the cortex. We found a marked increase of spine elimination and formation after 2 d in poly(I:C)-treated mice as compared to that in vehicle-treated controls (Supplementary Fig. 16). The relative increase in spine turnover after poly(I:C) administration was comparable between *Il6*$^{-/-}$→WT chimeras and WT mice, suggesting that increased amounts of IL-6 in the serum are not required for synaptic alteration in the cortex.

DISCUSSION

Despite the compelling evidence for an association between immune activation and cognitive disorders[4,5,6,7], the underlying mechanisms remain elusive. Here we identified an important role of CX_3CR1^+ monocytes and TNF-α in the modulation of learning-dependent synapse structural plasticity during peripheral immune activation (Supplementary Fig. 17). Specifically, we showed that the initiation of peripheral innate immunity with a viral mimetic increased postsynaptic dendritic spine turnover in the mouse motor cortex and decreased the dendritic spine formation associated with motor learning. These synaptic changes are prevented by the *in vivo* ablation of peripheral monocytes, but not by depletion of brain-resident microglial cells. By using BM chimeric mice and transgenic mice, we further showed that both synaptic and learning impairments require CX_3CR1^{high} blood monocytes and TNF-α production.

Because most dendritic spines in the adult cortex persist throughout life[28,29], the loss of dendritic spines after immune challenge is likely detrimental to the functions of synaptic networks. Previous studies have shown that motor-learning-dependent synapse formation strongly correlates with improvements in performance after learning[29,32]. Consistent with these studies, we observed a marked decrease in performance improvement after a period of rotarod learning in mice with impaired spine formation. Additionally, we observed that peripheral immune activation impaired the mouse's short- and long-term memory in NOR tasks. These results in mice resonate with clinical observations showing that patients with acute or chronic infectious diseases often have weaker performance on motor skills and experience memory decline relative to that in uninfected individuals [8, 9, 10, 11, 12, 13]. Furthermore, because immune activation is involved in many neuropsychiatric and neurological diseases[5, 6, 7], the synaptic abnormalities observed in our studies may also occur under these medical conditions and contribute to cognitive deficits.

Our findings underscore the importance of CX_3CR1^{high} monocytes for synaptic deficits and learning impairment during peripheral immune activation. This was demonstrated by a series of *in vivo* cell-depletion experiments using *Cx3cr1*$^{CreER/+}$;*R26*$^{iDTR/+}$ mice. First, immune-challenge-induced synaptic alteration could be prevented by the depletion of the entire CX_3CR1^+ population or by the ablation of CX_3CR1^{high} blood monocytes, but not by the removal of CNS microglia. Second, adoptive transfer of $CD11b^+$ cells, which include monocytes, reconstituted the phenotype in *Cx3cr1*$^{CreER/+}$;*R26*$^{iDTR/+}$ mice that were depleted of the entire CX_3CR1^+ population. Third, consistent with the finding that CX_3CR1-deficient mice have a reduced number of $Gr1^{low}$ (CX_3CR1^{high}) monocytes[45], mice with CX_3CR1 deficiency in peripheral leukocytes did not show synaptic and learning deficits during immune activation, further suggesting that CX_3CR1^{high} monocytes are essential for peripheral-immune-challenge-induced cortical changes.

CX_3CR1 is also expressed by human monocytes[44], in which CX_3CR1^{low} cells correspond to classical $CD14^+CD16^-$ monocytes, whereas nonclassical human $CD14^{low}CD16^+$ monocytes resemble mouse $CX_3CR1^{high}Ly6C^{low}$ blood-resident monocytes[52]. It has been shown that $CD14^{low}$ human monocytes patrol blood vessels in steady state and produce high amounts of TNFα and IL-1β in response to infection by the measles virus or herpes simplex virus (HSV-1) (ref. 52). In patients with an HIV infection, the $CD16^+$ monocyte subset preferentially harbors the virus[53] and activation of this subset is associated with neurocognitive impairment after viral infection[54,55]. Future studies of this monocytes population in humans will help explain their contribution to the cognitive decline associated with viral infection that is observed.

Our study links the activation of CX_3CR1^{high} monocytes to synaptic and learning deficits via TNF-α-dependent mechanisms. TNF-α can be produced by peripheral monocytes and endothelial cells, as well as by glia and neurons in the brain. Our studies strongly suggest that monocyte-dependent TNF-α production is a causative event in the initiation of dendritic spine alteration in the cortex (Supplementary Note 1). TNF-α may affect synaptic plasticity directly through neuronally expressed TNF receptor 1 (TNFR1)[47,48,49] and/or indirectly through astrocyte–neuron signaling[56] (Supplementary Note 2). Future use of genetic approaches to manipulate TNF signaling in specific cell types is needed to better understand how TNFα alters dendritic spine remodeling.

In summary, our present findings provide an important mechanism by which innate immune responses modulate the synapse structural plasticity associated with learning, which is likely relevant to cognitive disturbances that are associated with systemic infectious states, such as HIV-associated neurocognitive disorders, viral sepsis and meningitis. Targeting the human correlates of mouse $CX_3CR1^{high}Ly6C^{low}$ monocytes and preventing the production of TNF-α and synaptic deficits may be a potential therapeutic strategy to prevent cognitive disturbances in these medical conditions.

Methods

Mice

Thy1-YFP-H mice (stock 003782)[57], which express yellow fluorescent protein (YFP) in L5 pyramidal neurons, *Rosa26-stop-DTR* mice (stock 007900)[58], which express a conditional DTR-encoding allele in the ROSA locus, *Rag1*$^{-/-}$ mice (stock 002216)[59], *Tnf*$^{-/-}$ mice (stock 005540)[60], *Il6*$^{-/-}$ mice (stock 002650) and B6 CD45.1 mice (stock 002014) were purchased from the Jackson Laboratory. *Cx3cr1*^{CreER} mice[35] were obtained from the laboratory of Wen-Biao Gan (New York University). *Cx3cr1*^{GFP} mice[34] were obtained from the laboratory of Dan Littman (New York University). To image dendritic spine plasticity in *Cx3cr1*$^{CreER/+}$;*R26*$^{iDTR/+}$ and *Tnf*$^{-/-}$ mice, these mice were crossed to *Thy1*-YFP-H mice. For systemic immune challenge, mice were administered poly(I:C) (Sigma P1530; by i.p. injection) that was dissolved in DPBS. Mice were group-housed in temperature-controlled rooms on a 12-h light–dark cycle and were randomly assigned to different treatment groups. The group size was determined based on previous studies using the same methodologies[28,29,30,31,32]. Both male and female mice were used. All mice were maintained at the NYU Skirball Institute specific-pathogen-free animal facility and handled in accordance with the institutional guidelines for animal care and use.

In vivo cell depletion

For *in vivo* cell depletion, *Cx3cr1*$^{CreER/+}$ mice were used as non-depleted control, and *Cx3cr1*$^{CreER/+}$;*R26*$^{iDTR/+}$ mice were used for cell depletion. All mice (control and cell-depleted mice) were given both tamoxifen and diphtheria toxin. To induce CreER recombination, mice were administered tamoxifen (0.35 mg/g per day; oral gavage) dissolved in corn oil (Sigma) for 3 consecutive days. For cell depletion, diphtheria toxin (Sigma) was diluted in DPBS and 1 μg of toxin was given i.p. to adult mice (14–18 g body weight) for three consecutive days.

In vivo transcranial two-photon imaging

Dendritic spines in the cortex were imaged through a thinned-skull window using a two-photon microscope[27]. Briefly, surgical anesthesia was achieved using an intraperitoneal injection of 100 mg/kg ketamine and 15 mg/kg xylazine. A midline scalp incision exposed the skull. The area to be imaged was identified based on stereotaxic coordinates for the primary motor cortex (1 mm lateral from midline, 0.5 mm posterior from bregma). The head was immobilized, and a cranial window was created by thinning a circular area (~200 μm in diameter) of the skull to approximately 20 μm in thickness by using a high-speed drill and/or a microsurgical blade. Upon completion of the skull thinning, the animal was placed under a two-photon microscope while still under anesthesia. Two-photon laser was tuned to 920 nm. All experiments were performed using a 1.1 NA 60× objective immersed in artificial cerebrospinal fluid to obtain high-magnification (66.7 μm × 66.7 μm; 512 × 512 pixels; 0.75 μm step) images for dendritic spine analysis. After imaging, the scalp was sutured with 6–0 silk and the animal was returned to the home cage until the next viewing.

Imaging data analysis

Analysis of dendritic spine plasticity was performed using the NIH ImageJ software as described previously[28,29]. Briefly, for each dendritic segment, filopodia were identified as long, thin protrusions without bulbous heads and the remaining protrusions were classified as spines. Images of the same dendritic segments identified from two views were compared. Spines were considered stable if they were present in both views, eliminated if they were present in the 1st view but not in the 2nd view or newly formed if they were present in the 2nd view but not in the 1st view. The elimination and formation rates were measured as the number of spines eliminated or formed in the 2nd view divided by the number of spines existing in the 1st view. In some experiments (Fig. 2), after identification of new spines formed in the 2nd view, the persistence of new spines was determined by examining the image obtained from the 3rd view. The percentage of persistent new spines was measured as the number of new spines that were present in both 2nd and 3rd view, divided by the number of spines existing in the 1st view. For the analysis of spine morphology (Supplementary Fig. 1), eliminated or newly formed spines were classified into three categories: mushroom spines (bulbous head; neck length ≤ head diameter), thin spines (bulbous head; neck length > head diameter) and stubby spines (no visible neck).

To analyze microglial morphology, z-projections of confocal imaging stacks (100 μm × 100 μm × 15 μm) were generated using ImageJ software[61]. The percentage of area covered by microglia was calculated by making a binary image (Gray value 0 for background and 255 for GFP-labeled microglia) from the z-projection and counting the number of white pixels within the area. Investigators were blinded to experimental condition when performing data analysis.

Behavioral assays

All behavioral experiments were performed in double-blind fashion. Rotarod motor training was performed using an EZRod system. Animals were placed on a motorized rod (30 mm in diameter) in the test chamber (44.5 cm × 14 cm × 51 cm dimensions). The rod stayed stationary for 30 sec, and then the rotation speed linearly increased from 0 to 80 r. p. m. over the course of 2 min. The latency to fall and rotation speed were recorded when the animal was unable to keep up with the increasing speed. Rotarod training/testing was conducted in three 20-trial sessions per day over two consecutive days. Mice were tested again in two 20-trial sessions after 7 days. Performance was calculated as the average speed animals achieved during each day. The first training session started 24 h after vehicle or poly(I:C) injection.

For novel object recognition, mice were tested in custom-built opaque plexiglass boxes (25 cm × 25 cm × 25 cm). Behavior was videotaped using standard webcams and images were analyzed with Quicktime software (Apple). Mice were handled by the same researcher 2 min per day for 3 consecutive days and then habituated to the testing environment for 30 min with no objects in the chamber. Twenty four hours after the habituation, mice were placed into testing environment with two identical sample objects (the familiar object) placed in opposite corners for 10 min. Mice were removed and returned to their home cages. One or twenty four hours later, mice were returned to the testing environment for 5 min where one

of the sample objects was replaced by a novel object, which differs from the familiar object in the shape and texture. Testing session was scored by an experienced observer who was blinded to the experimental condition. Interaction with the familiar or novel object was considered to be the exploration time in which the animal spent with its head and nose oriented toward and within 2 cm of the object. Different types of interactions such as the animal accidentally touching, sitting or standing on the object were not considered exploratory activity. Discrimination ratio was calculated as the time spent exploring the novel object divided by the total time spent with both novel and familiar objects.

Cell isolation and flow cytometry

Mice were deeply anesthetized, and blood was collected from the retro-orbital vein. Mice were perfused with 25 ml of Ca^{2+}/Mg^{2+}-free DPBS (Sigma). Brain and liver were removed and placed in DPBS with 2% FCS. Single-cell suspensions from blood, liver and cortex were prepared. The liver was mechanically dissociated and filtered through 70-μm cell strainer. Cells were suspended in 40% Percoll layered over 80% Percoll for density centrifugation (2,000 r.p.m., 30 min). Enriched cells were collected from the interphase. The cortex was minced with scissors and incubated with 300 U of collagenase D (Roche, 11088858001) at 37 °C for 30 min. Collagenase was inactivated by adding 12.5 mM EDTA for an additional 5-min incubation at 37 °C. Digested material was passed through a 70-μM cell strainer, followed by a centrifugation at 2,000 r.p.m. in a continuous 38% Percoll gradient. Cell pellets were resuspended in FACS buffer (PBS containing 0.5% BSA, 1 mM EDTA and 0.05% sodium azide), and nonspecific binding to FC receptors was blocked by incubation with a CD16- and CD32-specific antibody (BioXcell, 2.4G2, 2.5 μg/ml) for 15 min. Cells were washed and stained with antibodies to the following proteins: CD11b (BioLegend, 101216, 1:400), CD45 (BioLegend, 103128, 1:200), CD45.1 (clone A20, 1:200), CD45.2 (clone 104, 1:200), Ly6C (BioLegend, 128011, 1:1,000) and a lineage-specific antibody cocktail (LIN: CD19 (BioLegend, 152407, 1:200), CD3 (BioLegend, 100307, 1:200), TCR-β chain (BioLegend, 109207, 1:200)). Flow cytometry was performed on an LSRII (BD) and analyzed with FlowJo v. 8.7 (Treestar).

BM chimera generation

One-month-old recipient mice (10–12 g) were exposed to 1,200 rad of whole-body gamma irradiation in 2 sessions of 7.5 min, 3 h apart. Head protection was used in separate cohorts of recipient mice during irradiation to exclude the potential artifacts caused by cranial irradiation. Recipient mice were injected with donor BM cells ($3–5 \times 10^6$ cells) through the retro-orbital venous sinus 1–3 h after the second session of irradiation. Donor BM cells were extracted from the femur of donor mice and passed through a 70-μm cell strainer. Animals' body weight was monitored every other day. For the first 2 weeks after irradiation, animals' drinking water was supplemented with 2 mg/ml sulfamethoxazole and 0.4 mg/ml trimethoprim. Four to six weeks after BM reconstitution, most of BM chimeric mice (from all genotypes tested) were healthy (normal body weight, gait and absence of clasping reflex) and exhibited normal motor function and a preference for the novel object in the NOR test. Flow cytometry analysis from blood samples of congenic (CD45.1→CD45.2) chimeras confirmed that 75 ± 10 % (n = 2 mice) of circulating leukocytes were of donor origin 4–6 weeks after BM reconstitution.

Previous study suggests that cranial irradiation may harm blood-brain barrier and cause recruitment of BM cells into the CNS parenchyma[39,62]. To examine the possibility that BM cells may be recruited into the motor cortex of irradiated mice, we generated chimeric mice with *Cx3cr1*$^{GFP/+}$ BM and examined the mouse cortex using 2-photon microscopy. One month after BM transplantation, we did not observe GFP-expressing cells in the parenchyma of the motor cortex, indicating limited parenchymal recruitment of BM cells into the cortex during the time window relevant to the current study. Moreover, we found no significant differences in dendritic spine plasticity and motor performance between head-protected chimeric animals and chimeras without head protection during irradiation (Supplementary Figs. 7 and 15).

Magnetic cell sorting

CD11b$^+$ cells were harvested from the blood and spleen by magnetic cell sorting. Blood was collected from anesthetized mice through the retro-orbital vein using heparinized capillary tubes and then diluted in DPBS (1:1 vol/vol). Leukocytes were isolated by centrifugation in an iso-osmotic polysucrose and diatrizoate solution (lymphocyte separation medium; Corning) at 300*g* for 30 min at 4 °C. For the isolation of splenocytes, spleens from anesthetized mice were dissected and smashed in magnetic cell sorting (MACS) buffer containing 0.5% BSA and 2 mM EDTA in PBS, pH 7.2, at 4 °C. The cell suspension was passed through a 70-μm cell strainer, centrifuged at 300*g* for 10 min at 4 °C, resuspended in ACK lysis buffer (Lonza) for 3 min and then washed in MACS buffer. Blood and spleen leukocytes were resuspended in 400 μl of MACS buffer and incubated with 40 μl of CD11b Microbeads (Miltenyi Biotec) for 15 min at 4 °C. Magnetic separation was performed in appropriate MACS separators. Cell viability was evaluated by a trypan blue exclusion assay, in which cells were incubated in 0.4% trypan blue in isotonic salt solution and evaluated in a hemocytometer. Sorted CD11b$^+$ cells were transferred to the recipient mice through the retro-orbital vein.

Immunohistochemistry

Mice were deeply anesthetized and perfused with 20 ml Ca^{2+}/Mg^{2+}-free DPBS. The brain was removed and fixed overnight in 4% paraformaldehyde at 4°C. The tissue was rinsed three times with PBS and sectioned at 200 μm with a Leica vibratome (VT 1000 S). Sections were permeabilized in 1% Triton X-100 in PBS for at least 3 h and blocked with a solution containing 0.1% Triton X-100 and 5% normal goat serum for 1 h. Sections were incubated overnight with primary antibodies: rabbit anti-Iba1 (Wako 019-19741, 1:300), chicken anti-GFAP (Millipore AB5541, 1:200), mouse anti-NeuN (Millipore MAB377, 1:200), or rat anti-TNF-α (Biolegend 506302, 1:50). Sections were then washed three times with 0.05% Tween-20 in PBS and then incubated for 1 h with the appropriate secondary antibodies: Alexa-Fluor-405-conjugated goat anti-rat IgG (Abcam 175671); Alexa-Fluor-647-conjugated goat anti-rabbit-IgG (Invitrogen A32733) or goat anti-mouse-IgG (Invitrogen A21236). Sections were washed as described before, incubated with or without DAPI (1 ng/ml) for 10 min, washed and mounted in MoWiol 4–88/glycerol for imaging. For the double staining of TNF-α and the neuronal marker NeuN, sections were pre-treated with sodium citrate buffer (10 mM sodium citrate, 0.05% Tween 20, pH, 5.8) and heated at 100°C

for 3 min before proceeding with the procedure described above. Confocal images were obtained on a Zeiss 700 confocal microscope.

ELISA

Whole blood was collected by ventricular puncture while mice were under deep anesthesia. Blood samples were centrifuged at 1400 *g* for 10 min to generate plasma fractions. Brain samples were prepared in separate experiments, in which mice were perfused with 25 ml of Ca^{2+}/Mg^{2+}-free DPBS to remove remaining blood. CNS tissues were harvested and disrupted by sonication in NP-40 lysis buffer (50 mM Tris pH=7.4, 150 mM NaCl, 1% NP-40, 0.1% Triton X-100, and 0.1% SDS) containing protease inhibitors (Thermo Scientific). The homogenized material was centrifuged at 20,000 *g* for 15 min and the cleared supernatant was collected for analysis. Total protein levels in CNS homogenates were determined by BCA assay (Pierce). TNFα, IL-6 and IL-1β protein levels were measured using the Mouse Platinum ELISA kit (eBioscience), and IFNβ was measured using the Mouse IFNβ ELISA kit (Life Technologies). Samples were processed according to the manufacturer's instructions.

Statistics

Prism software (GraphPad 6.0, La Jolla, CA) was used to conduct the statistical analysis. Summary data were presented as mean ± s.e.m. Tests for differences between two populations were performed using Mann-Whitney test or Wilcoxon test. Multiple group comparison was performed with nonparametric Kruskal-Wallis test or one-way ANOVA followed by a Bonferroni's *post hoc* test as specified in the figure legends. No data points were excluded from the statistical analysis, and variance was similar between groups being statistically compared. Significant levels were set at $P < 0.05$.

Supplementary Material

Refer to Web version on PubMed Central for supplementary material.

Acknowledgments

We thank W.B. Gan (New York University) from providing *Cx3cr1*-CreER mice, D.R. Littman (New York University) for providing *Cx3cr1*-GFP mice. We also thank W.B. Gan and M.V. Bennett for critical reading of the manuscript. This work was supported by Whitehall Foundation Research Grant (G.Y.), National Institutes of Health grants R01 GM107469 and R21 AG048410 (G.Y.), and CNPq fellowship-Brazil (H.M.S.).

References

1. Yirmiya R, Goshen I. Immune modulation of learning, memory, neural plasticity and neurogenesis. Brain Behav Immun. 2011; 25:181–213. [PubMed: 20970492]
2. Ransohoff RM, Engelhardt B. The anatomical and cellular basis of immune surveillance in the central nervous system. Nat Rev Immunol. 2012; 12:623–635. [PubMed: 22903150]
3. Marin I, Kipnis J. Learning and memory … and the immune system. Learn Memory. 2013; 20:601–606.
4. Hodes GE, Kana V, Menard C, Merad M, Russo SJ. Neuroimmune mechanisms of depression. Nat Neurosci. 2015; 18:1386–1393. [PubMed: 26404713]
5. Perry VH, Cunningham C, Holmes C. Systemic infections and inflammation affect chronic neurodegeneration. Nat Rev Immunol. 2007; 7:161–167. [PubMed: 17220915]

6. Brown AS, Derkits EJ. Prenatal infection and schizophrenia: a review of epidemiologic and translational studies. The American journal of psychiatry. 2010; 167:261–280. [PubMed: 20123911]
7. Estes ML, McAllister AK. Immune mediators in the brain and peripheral tissues in autism spectrum disorder. Nat Rev Neurosci. 2015; 16:469–486. [PubMed: 26189694]
8. Schmidt H, et al. Neuropsychological sequelae of bacterial and viral meningitis. Brain. 2006; 129:333–345. [PubMed: 16364957]
9. Bucks RS, et al. Selective effects of upper respiratory tract infection on cognition, mood and emotion processing: A prospective study. Brain Behavior and Immunity. 2008; 22:399–407.
10. Thomas P, et al. Exposure to herpes simplex virus, type 1 and reduced cognitive function. Journal of psychiatric research. 2013; 47:1680–1685. [PubMed: 23920011]
11. Clifford DB, Ances BM. HIV-associated neurocognitive disorder. Lancet Infect Dis. 2013; 13:976–986. [PubMed: 24156898]
12. Hilsabeck RC, Perry W, Hassanein TI. Neuropsychological impairment in patients with chronic hepatitis C. Hepatology. 2002; 35:440–446. [PubMed: 11826421]
13. Sadek JR, et al. Persistent neuropsychological impairment associated with West Nile virus infection. Journal of clinical and experimental neuropsychology. 2010; 32:81–87. [PubMed: 19513920]
14. Meyer U. Prenatal poly(i:C) exposure and other developmental immune activation models in rodent systems. Biol Psychiatry. 2014; 75:307–315. [PubMed: 23938317]
15. Majde JA. Viral double-stranded RNA, cytokines, and the flu. Journal of interferon & cytokine research : the official journal of the International Society for Interferon and Cytokine Research. 2000; 20:259–272.
16. Alexopoulou L, Holt AC, Medzhitov R, Flavell RA. Recognition of double-stranded RNA and activation of NF-kappaB by Toll-like receptor 3. Nature. 2001; 413:732–738. [PubMed: 11607032]
17. Konat G. Cerebral Response to Peripheral Challenge with a Viral Mimetic. Neurochem Res. 2016; 41:144–155. [PubMed: 26526143]
18. Cunningham C, Campion S, Teeling J, Felton L, Perry VH. The sickness behaviour and CNS inflammatory mediator profile induced by systemic challenge of mice with synthetic double-stranded RNA (poly I:C). Brain Behav Immun. 2007; 21:490–502. [PubMed: 17321719]
19. Ibi D, et al. Neonatal polyI:C treatment in mice results in schizophrenia-like behavioral and neurochemical abnormalities in adulthood. Neuroscience research. 2009; 64:297–305. [PubMed: 19447299]
20. Kranjac D, et al. Peripheral administration of poly I:C disrupts contextual fear memory consolidation and BDNF expression in mice. Behav Brain Res. 2012; 228:452–457. [PubMed: 22222172]
21. Blank T, et al. Brain Endothelial- and Epithelial-Specific Interferon Receptor Chain 1 Drives Virus-Induced Sickness Behavior and Cognitive Impairment. Immunity. 2016; 44:901–912. [PubMed: 27096319]
22. Auffray C, Sieweke MH, Geissmann F. Blood monocytes: development, heterogeneity, and relationship with dendritic cells. Annual review of immunology. 2009; 27:669–692.
23. Shi C, Pamer EG. Monocyte recruitment during infection and inflammation. Nat Rev Immunol. 2011; 11:762–774. [PubMed: 21984070]
24. Auffray C, et al. Monitoring of blood vessels and tissues by a population of monocytes with patrolling behavior. Science. 2007; 317:666–670. [PubMed: 17673663]
25. Kim JV, Kang SS, Dustin ML, McGavern DB. Myelomonocytic cell recruitment causes fatal CNS vascular injury during acute viral meningitis. Nature. 2009; 457:191–195. [PubMed: 19011611]
26. Rivest S. Regulation of innate immune responses in the brain. Nat Rev Immunol. 2009; 9:429–439. [PubMed: 19461673]
27. Yang G, Pan F, Parkhurst CN, Grutzendler J, Gan WB. Thinned-skull cranial window technique for long-term imaging of the cortex in live mice. Nat Protoc. 2010; 5:201–208. [PubMed: 20134419]
28. Grutzendler J, Kasthuri N, Gan WB. Long-term dendritic spine stability in the adult cortex. Nature. 2002; 420:812–816. [PubMed: 12490949]

29. Yang G, Pan F, Gan WB. Stably maintained dendritic spines are associated with lifelong memories. Nature. 2009; 462:920–924. [PubMed: 19946265]
30. Xu T, et al. Rapid formation and selective stabilization of synapses for enduring motor memories. Nature. 2009; 462:915–919. [PubMed: 19946267]
31. Lai CS, Franke TF, Gan WB. Opposite effects of fear conditioning and extinction on dendritic spine remodelling. Nature. 2012; 483:87–91. [PubMed: 22343895]
32. Liston C, et al. Circadian glucocorticoid oscillations promote learning-dependent synapse formation and maintenance. Nat Neurosci. 2013; 16:698–705. [PubMed: 23624512]
33. Hayashi-Takagi A, et al. Labelling and optical erasure of synaptic memory traces in the motor cortex. Nature. 2015; 525:333–338. [PubMed: 26352471]
34. Jung S, et al. Analysis of fractalkine receptor CX(3)CR1 function by targeted deletion and green fluorescent protein reporter gene insertion. Molecular and cellular biology. 2000; 20:4106–4114. [PubMed: 10805752]
35. Parkhurst CN, et al. Microglia promote learning-dependent synapse formation through brain-derived neurotrophic factor. Cell. 2013; 155:1596–1609. [PubMed: 24360280]
36. Schafer DP, et al. Microglia sculpt postnatal neural circuits in an activity and complement-dependent manner. Neuron. 2012; 74:691–705. [PubMed: 22632727]
37. Hong S, et al. Complement and microglia mediate early synapse loss in Alzheimer mouse models. Science. 2016
38. Goldmann T, et al. Origin, fate and dynamics of macrophages at central nervous system interfaces. Nature immunology. 2016; 17:797-+. [PubMed: 27135602]
39. Ajami B, Bennett JL, Krieger C, Tetzlaff W, Rossi FMV. Local self-renewal can sustain CNS microglia maintenance and function throughout adult life. Nature Neuroscience. 2007; 10:1538–1543. [PubMed: 18026097]
40. Lawson LJ, Perry VH, Gordon S. Turnover of resident microglia in the normal adult mouse brain. Neuroscience. 1992; 48:405–415. [PubMed: 1603325]
41. Ginhoux F, et al. Fate Mapping Analysis Reveals That Adult Microglia Derive from Primitive Macrophages. Science. 2010; 330:841–845. [PubMed: 20966214]
42. van Furth R, Cohn ZA. The origin and kinetics of mononuclear phagocytes. J Exp Med. 1968; 128:415–435. [PubMed: 5666958]
43. Yona S, et al. Fate mapping reveals origins and dynamics of monocytes and tissue macrophages under homeostasis. Immunity. 2013; 38:79–91. [PubMed: 23273845]
44. Geissmann F, Jung S, Littman DR. Blood monocytes consist of two principal subsets with distinct migratory properties. Immunity. 2003; 19:71–82. [PubMed: 12871640]
45. Landsman L, et al. CX3CR1 is required for monocyte homeostasis and atherogenesis by promoting cell survival. Blood. 2009; 113:963–972. [PubMed: 18971423]
46. Yang G, Parkhurst CN, Hayes S, Gan WB. Peripheral elevation of TNF-alpha leads to early synaptic abnormalities in the mouse somatosensory cortex in experimental autoimmune encephalomyelitis. Proc Natl Acad Sci U S A. 2013
47. Beattie EC, et al. Control of synaptic strength by glial TNF alpha. Science. 2002; 295:2282–2285. [PubMed: 11910117]
48. Stellwagen D, Malenka RC. Synaptic scaling mediated by glial TNF-alpha. Nature. 2006; 440:1054–1059. [PubMed: 16547515]
49. Stellwagen D, Beattie EC, Seo JY, Malenka RC. Differential regulation of AMPA receptor and GABA receptor trafficking by tumor necrosis factor-alpha. Journal of Neuroscience. 2005; 25:3219–3228. [PubMed: 15788779]
50. Obermeier B, Daneman R, Ransohoff RM. Development, maintenance and disruption of the blood-brain barrier. Nat Med. 2013; 19:1584–1596. [PubMed: 24309662]
51. Gu Z, et al. A highly specific inhibitor of matrix metalloproteinase-9 rescues laminin from proteolysis and neurons from apoptosis in transient focal cerebral ischemia. J Neurosci. 2005; 25:6401–6408. [PubMed: 16000631]
52. Cros J, et al. Human CD14dim monocytes patrol and sense nucleic acids and viruses via TLR7 and TLR8 receptors. Immunity. 2010; 33:375–386. [PubMed: 20832340]

53. Ellery PJ, et al. The CD16+ monocyte subset is more permissive to infection and preferentially harbors HIV-1 in vivo. J Immunol. 2007; 178:6581–6589. [PubMed: 17475889]

54. Williams DW, et al. Monocytes Mediate HIV Neuropathogenesis: Mechanisms that Contribute to HIV Associated Neurocognitive Disorders. Curr Hiv Res. 2014; 12:85–96. [PubMed: 24862333]

55. Imp BM, et al. Monocyte Activation Is Associated With Worse Cognitive Performance in HIV-Infected Women With Virologic Suppression. The Journal of infectious diseases. 2017; 215:114–121. [PubMed: 27789726]

56. Habbas S, et al. Neuroinflammatory TNFalpha Impairs Memory via Astrocyte Signaling. Cell. 2015; 163:1730–1741. [PubMed: 26686654]

57. Feng G, et al. Imaging neuronal subsets in transgenic mice expressing multiple spectral variants of GFP. Neuron. 2000; 28:41–51. [PubMed: 11086982]

58. Buch T, et al. A Cre-inducible diphtheria toxin receptor mediates cell lineage ablation after toxin administration. Nature methods. 2005; 2:419–426. [PubMed: 15908920]

59. Mombaerts P, et al. Rag-1-Deficient Mice Have No Mature Lymphocytes-B and Lymphocytes-T. Cell. 1992; 68:869–877. [PubMed: 1547488]

60. Pasparakis M, Alexopoulou L, Episkopou V, Kollias G. Immune and inflammatory responses in TNF alpha-deficient mice: a critical requirement for TNF alpha in the formation of primary B cell follicles, follicular dendritic cell networks and germinal centers, and in the maturation of the humoral immune response. J Exp Med. 1996; 184:1397–1411. [PubMed: 8879212]

61. Garre JM, Yang G, Bukauskas FF, Bennett MV. FGF-1 Triggers Pannexin-1 Hemichannel Opening in Spinal Astrocytes of Rodents and Promotes Inflammatory Responses in Acute Spinal Cord Slices. J Neurosci. 2016; 36:4785–4801. [PubMed: 27122036]

62. Mildner A, et al. Microglia in the adult brain arise from Ly-6ChiCCR2+ monocytes only under defined host conditions. Nat Neurosci. 2007; 10:1544–1553. [PubMed: 18026096]

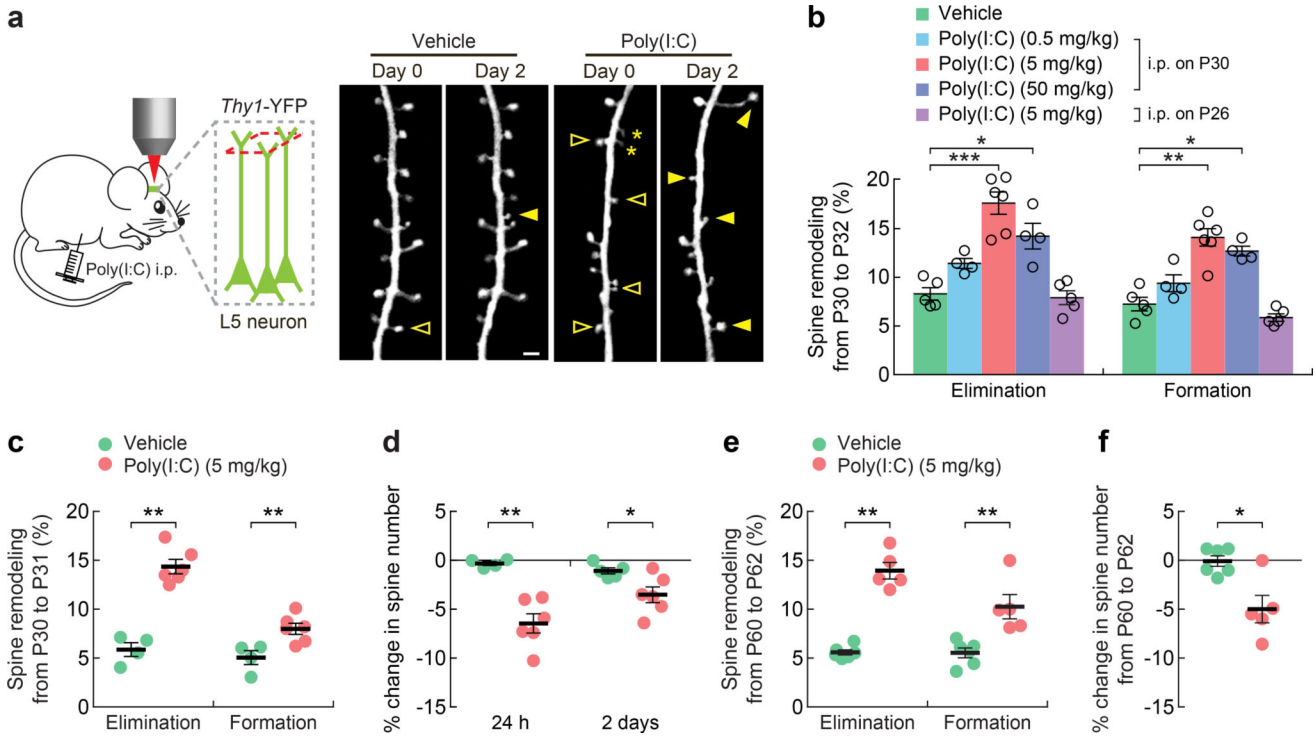

Figure 1. Systemic immune challenge increases dendritic spine turnover in the cortex

(**a**) Left, cartoon depicting the experimental approach for longitudinal imaging of synaptic structural plasticity in Thy1-YFP transgenic mice, which express yellow fluorescent protein (YFP) in L5 pyramidal neurons. Right, representative images of transcranial two-photon imaging of dendritic spines on apical dendritic segments of L5 pyramidal neurons in the primary motor cortex of vehicle- or poly(I:C)-treated mice. Empty and filled arrowheads indicate individual spines that were eliminated or newly formed, respectively, on the same dendritic segment after 2 d. Asterisks indicate dendritic filopodia. Scale bar, 2 μm. (**b**) Summary quantification of dendritic spine elimination and formation from P30 to P32 in mice that were injected with a vehicle solution ($n = 5$ mice), with 0.5 mg/kg ($n = 4$ mice), 5 mg/kg ($n = 6$ mice) or 50 mg/kg ($n = 4$ mice) poly(I:C) i.p. at P30 or with 5 mg/kg poly(I:C) at P26 ($n = 5$ mice). (**c**) Spine elimination and formation 24 h after vehicle ($n = 4$ mice) or poly(I:C) ($n = 6$ mice) injection. (**d**) Net change in spine number after vehicle or poly(I:C) injection at P30 for the mice in c. (**e**) Quantification of dendritic spine elimination and formation after 2 d in mice that were injected with vehicle ($n = 6$ mice) or 5 mg/kg poly(I:C) ($n = 5$ mice) at P60. (**f**) Net change in spine number after 2 d in the vehicle- or poly(I:C)-treated mice in e. Throughout, individual circles represent data from a single mouse. Summary data are presented as mean ± s.e.m. $*P < 0.05$, $**P < 0.01$, $***P < 0.001$; by the Kruskal–Wallis (**b**) or Mann–Whitney (**c–f**) test. See also Supplementary Table 1.

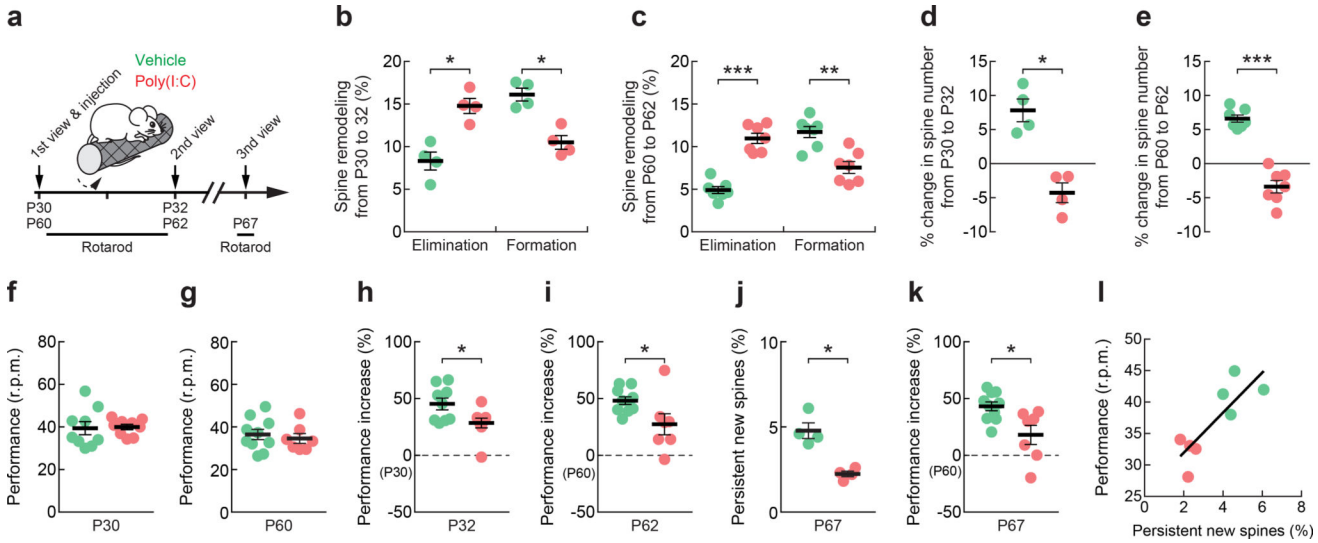

Figure 2. Systemic immune challenge impairs learning-dependent spine remodeling and performance improvement

(**a**) Schematic showing the timeline for *in vivo* imaging, vehicle or poly(I:C) (5 mg/kg i.p.) administration, and rotarod training and testing. (**b,c**) Effect of poly(I:C) treatment on dendritic spine elimination and formation after a 2-d rotarod training period in P30 ($n = 4$ mice per group) (**b**) or P60 ($n = 7$ mice per group) (**c**) mice. (**d,e**) Net change in spine number after a 2-d rotarod training period in the P30 (**d**) and P60 (**e**) mice in **b,c**, respectively. (**f,g**) Effect of poly(I:C) treatment on baseline rotarod performance in P30 ($n = 9$ mice per group) (**f**) and P60 (vehicle-treated, $n = 10$ mice; poly(I:C)-treated, $n = 7$ mice) (**g**) mice. Rotarod performance is expressed as the average speed reached during the training day. (**h,i**) Rotarod performance improvement assessed after 2 d for the mice that were treated at P30 (**h**) or P60 (**i**) in **f,g**, respectively. (**j**) Number of persistent new spines in mice that were injected with vehicle ($n = 4$) or poly(I:C) ($n = 4$). Persistent new spines are expressed as the number of new spines formed during the 2-d training period (P60 to P62) that persist on P67, as a percentage of the total number of spines quantified at P60. (**k**) Rotarod performance improvement, as assessed at P67, for the mice in g. (**l**) Correlation between the number of persistent new spines and the mouse's rotarod performance on P67 ($r = 0.7857$; $P = 0.0279$; by Spearman correlation). Throughout, individual circles represent data from a single mouse. Summary data are presented as mean ± s.e.m. $^{*}P < 0.05$, $^{**}P < 0.01$, $^{***}P < 0.001$; by Mann–Whitney test. See also Supplementary Table 1.

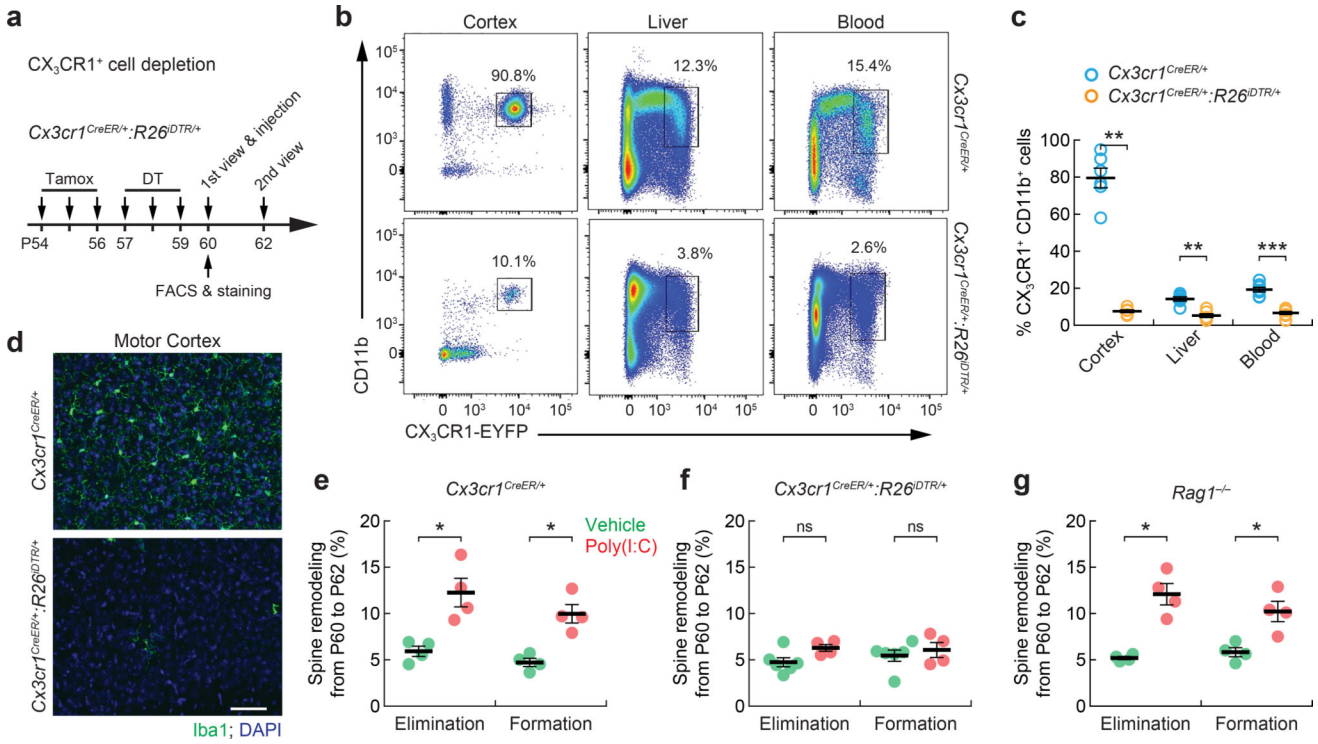

Figure 3. CX_3CR1^+ cells are required for altered dendritic spine plasticity after systemic immune challenge

(**a**) Schematic representation of the strategy to deplete CX_3CR1^+ cells, which include peripheral monocytes and CNS-resident microglia. (**b**) Representative flow cytometry analysis showing the percentages of CX_3CR1–$EYFP^+CD11b^+$ cells in the cortex (left), liver (middle) and blood (right) of *Cx3cr1*$^{CreER/+}$ (top) or *Cx3cr1*$^{CreER/+}$;*R26*$^{iDTR/+}$ (bottom) mice after administration of the last dose of DT. Gate: singlets, $DAPI^-LIN^-CD45^{low}$ (cortex) or $CD45^{high}$ (periphery). (**c**) Quantification of the data shown in **b** ($n = 6$ mice for each group). (**d**) Representative coronal sections ($n = 8$ sections per group) of the motor cortex from control (top) and CX_3CR1^+-cell-depleted (bottom) mice that were stained with the microglia marker Iba1 1 d after administration of the last dose of DT. Scale bar, 50 μm. (**e**) Quantification of dendritic spine elimination and formation over 2 d in *Cx3cr1*$^{CreER/+}$ control mice that were injected with vehicle or poly(I:C) ($n = 4$ mice per group). (**f**) Dendritic spine elimination and formation after 2 d in *Cx3cr1*$^{CreER/+}$;*R26*$^{iDTR/+}$ mice (which are depleted of CX_3CR1^+ cells) that were injected with vehicle ($n = 6$ mice) or poly(I:C) ($n = 4$ mice). (**g**) Dendritic spine elimination and formation after 2 d in *Rag1*$^{-/-}$ mice that were injected with vehicle or poly(I:C) ($n = 4$ mice per group). Throughout, individual circles represent data from a single mouse. Summary data are presented as mean ± s.e.m. $^*P < 0.05$, $^{**}P < 0.01$, $^{***}P < 0.001$; n.s., not significant; by Mann–Whitney test. See also Supplementary Table 1.

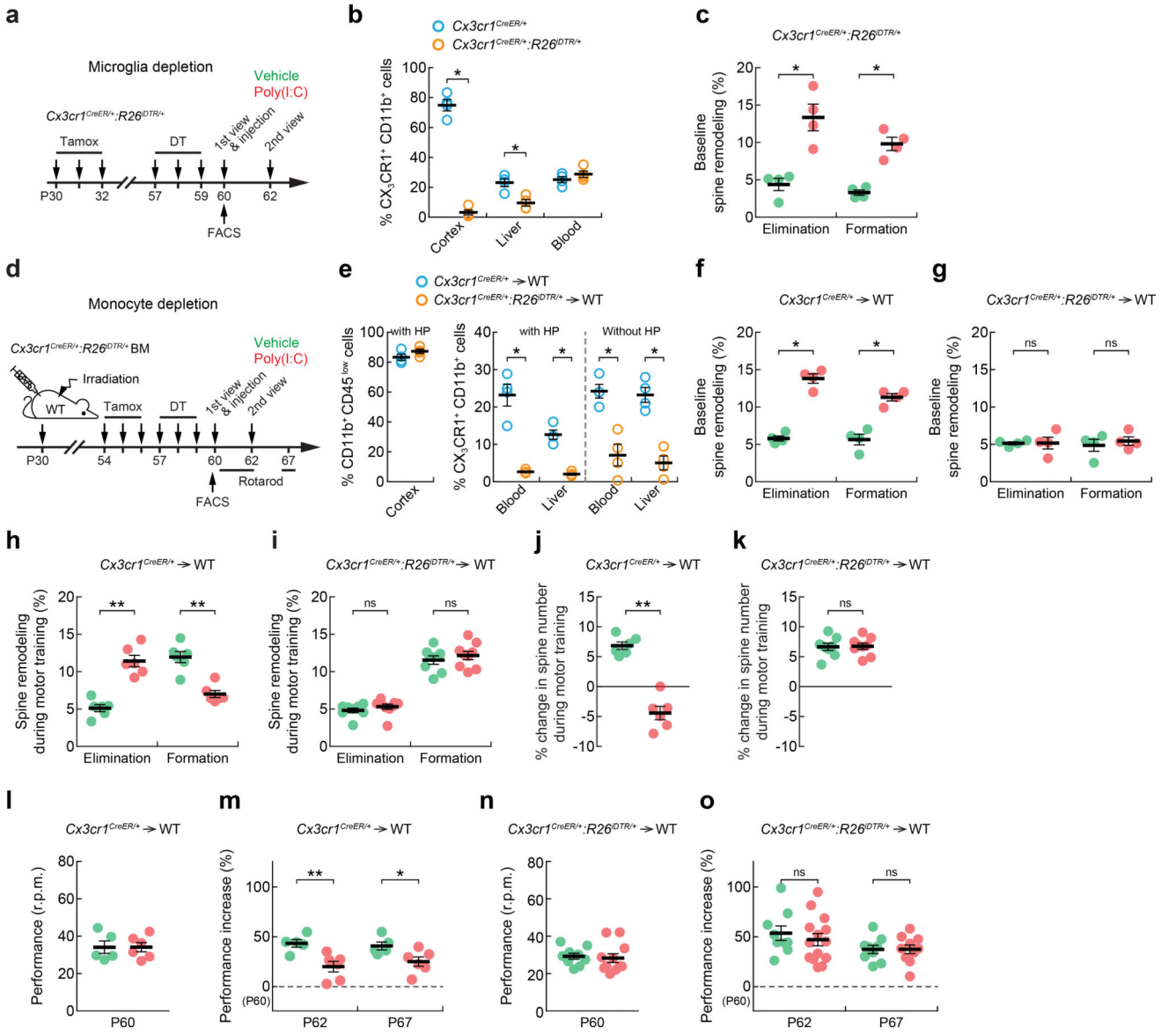

Figure 4. CX_3CR1^+ monocytes, but not microglia, mediate synaptic and learning deficits after systemic immune challenge

(**a**) Schematic of the strategy to selectively deplete CNS-resident microglia. (**b**) Quantification of $CX_3CR1^+CD11b^+$ cells in the cortex, liver and blood of *Cx3cr1*$^{CreER/+}$ (control) or *Cx3cr1*$^{CreER/+}$;*R26*$^{iDTR/+}$ mice 1 d after administration of the last dose of DT (n = 4 mice per group). (**c**) Effect of poly(I:C) treatment on dendritic spine elimination and formation after 2 d in *Cx3cr1*$^{CreER/+}$;*R26*$^{iDTR/+}$ mice that were depleted of microglia (n = 4 mice per group). (**d**) Schematic of the strategy to selectively deplete CX_3CR1^+ monocytes using *Cx3cr1*$^{CreER/+}$;*R26*$^{iDTR/+}$→WT chimeras. *Cx3cr1*$^{CreER/+}$→WT chimeras were used as controls. Irradiation was performed with or without head protection (HP). (**e**) Percentages of $CD11b^+CD45^{low}$ cells (microglia) in the cortex and $CX_3CR1^+CD11b^+$ cells in blood and liver after administration of the last DT injection (n = 4 mice per group). (**f,g**) Effect of poly(I:C) treatment on baseline spine elimination and formation after 2 d in

Cx3cr1$^{CreER/+}$→WT (**f**) or *Cx3cr1*$^{CreER/+}$;*R26*$^{iDTR/+}$→WT (**g**) chimeras (n = 4 mice per group). (**h,i**) Effect of poly(I:C) treatment on dendritic spine elimination and formation after a 2-d motor-training period in *Cx3cr1*$^{CreER/+}$→WT (n = 6 mice per group) (**h**) or in *Cx3cr1*$^{CreER/+}$;*R26*$^{iDTR/+}$→WT chimeras (vehicle-treated, n = 8; poly(I:C)-treated, n = 9 mice) (**i**). (**j,k**) Net change in spine number after a 2-d motor-training period for the mice in h (**j**) and i (**k**). (**l–o**) Effect of poly(I:C) treatment on rotarod performance in *Cx3cr1*$^{CreER/+}$→WT (vehicle-treated, n = 5 mice; poly(I:C)-treated, n = 6 mice) (**l,m**) or in *Cx3cr1*$^{CreER/+}$;*R26*$^{iDTR/+}$→WT chimeras (vehicle-treated, n = 9 mice; poly(I:C)-treated, n = 11 mice) (**n,o**) that were injected with vehicle or poly(I:C) on P60. Throughout, individual circles represent data from a single mouse. Summary data are presented as mean ± s.e.m. *P < 0.05, **P < 0.01; n.s., not significant; by Mann–Whitney test. See also Supplementary Table 1.

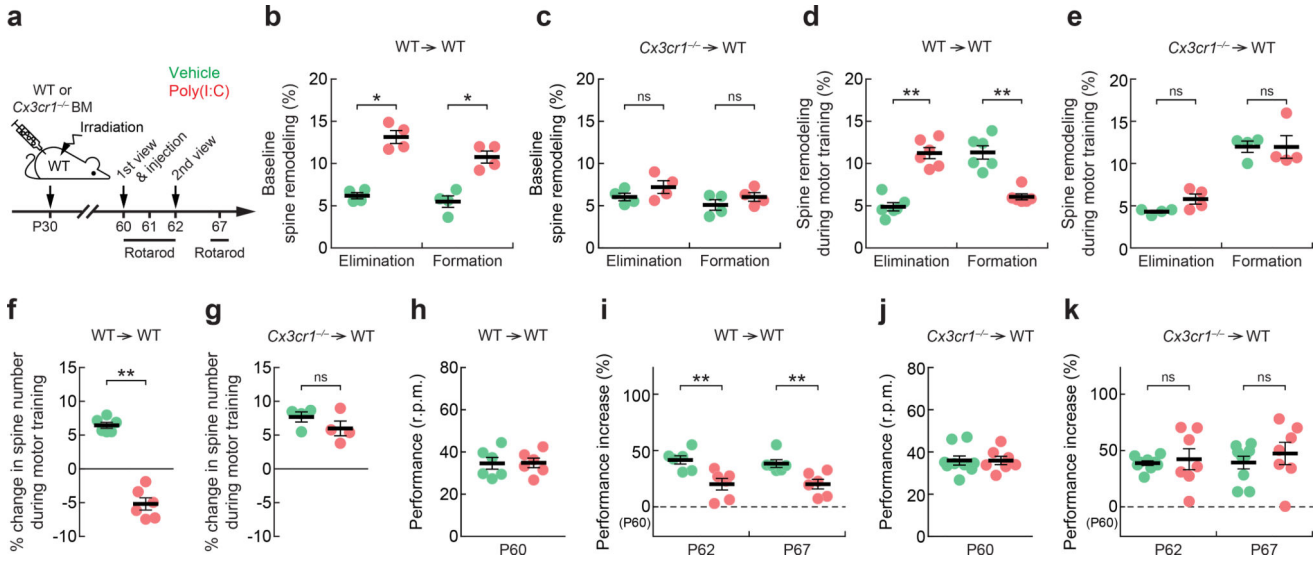

Figure 5. *Cx3cr1*$^{-/-}$ chimeric mice do not show synaptic and learning deficits during systemic immune challenge

(**a**) Schematic showing the timeline of BM chimera generation, vehicle or poly(I:C) (5 mg/kg i.p.) administration, rotarod training and *in vivo* two-photon imaging. (**b,c**) Effect of poly(I:C) treatment on baseline spine elimination and formation after 2 d in WT→WT (**b**) or *Cx3cr1*$^{-/-}$→WT (c) chimeras (n = 4 mice per group). (**d,e**) Effect of poly(I:C) treatment on dendritic spine elimination and formation after a 2-d motor-training period in WT→WT (n = 6 mice per group) (**d**) or *Cx3cr1*$^{-/-}$→WT chimeras (n = 4 mice per group) (**e**). (**f,g**) Net change in total spine numbers after a 2-d motor-training period in WT→WT (**f**) or *Cx3cr1*$^{-/-}$→WT (**g**) chimeras. (**h–k**) Effect of poly(I:C) administration on rotarod performance in WT→WT (n = 6 mice per group) (**h,i**) or *Cx3cr1*$^{-/-}$→WT (vehicle-treated, n = 9 mice; poly(I:C)-treated, n = 7 mice) (**j,k**) chimeras. Throughout, individual circles represent data from a single mouse. Summary data are presented as mean ± s.e.m. *P < 0.05, **P < 0.01; n.s., not significant; by Mann–Whitney test. See also Supplementary Table 1.

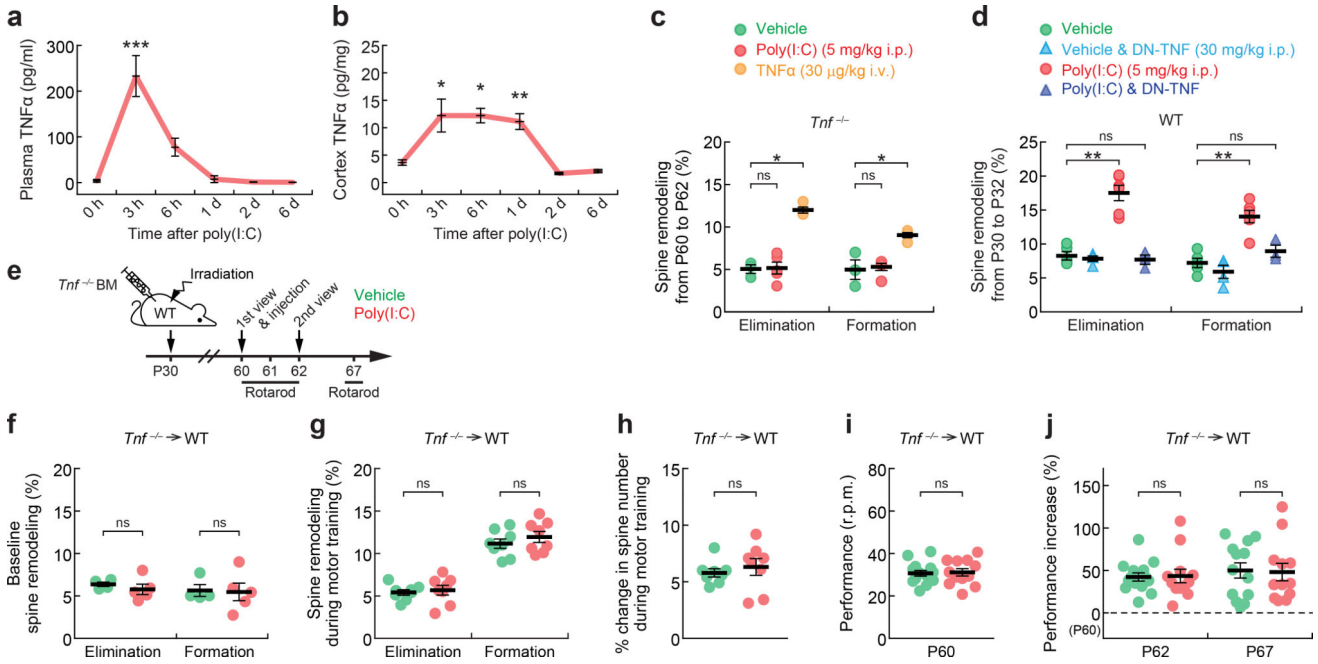

Figure 6. TNF-α mediates synaptic and learning deficits after systemic immune challenge

(**a,b**) Levels of TNF-α in the plasma ($F_{3,14}$ = 23.37, P < 0.0001) (**a**) or cortex ($F_{3,26}$ = 5.717, P = 0.0038) (**b**) of WT mice over time after injection with 5 mg/kg poly(I:C). (**c**) Summary quantification of dendritic spine remodeling after 2 d (imaged at P60 and P62) in *Tnf*$^{-/-}$ mice that were injected with vehicle (n = 3 mice), 5 mg/kg poly(I:C) (n = 5 mice) or 30 μg/kg exogenous TNF-α (n = 4 mice). (**d**) Summary quantification of dendritic spine elimination and formation after 2 d (imaged at P30 and P32) in WT mice that were injected with vehicle (n = 5 mice), 30 mg/kg DN-TNF (n = 4 mice), 5 mg/kg poly(I:C) (n = 6 mice), or poly(I:C) + DN-TNF (n = 3 mice). (**e**) Schematic of the timeline of bone marrow (BM) chimera generation, vehicle or poly(I:C) (5 mg/kg i.p.) injection, rotarod training and *in vivo* two-photon imaging. (**f**) Baseline spine elimination and formation after 2 d in *Tnf*$^{-/-}$→WT chimeras that were injected with vehicle (n = 4 mice) or poly(I:C) (n = 5 mice). (**g, h**) Effect of poly(I:C) treatment on dendritic spine remodeling (**g**) or total spine number (**h**) after a 2-d motor-training period in *Tnf*$^{-/-}$→WT chimeras (n = 8 mice per group). (**i,j**) Rotarod performance in *Tnf*$^{-/-}$→WT chimeras that were injected with vehicle (n = 14 mice) or poly(I:C) (n = 12 mice) at the time of injection (**i**) or after a 2-d motor-training period (**j**). Throughout, individual circles represent data from a single mouse. Summary data are presented as mean ± s.e.m. *P < 0.05, **P < 0.01, ***P < 0.001; n.s., not significant; by one-way analysis of variance (ANOVA) and post hoc Bonferroni (**a,b**), Kruskal–Wallis (**c,d**) or Mann–Whitney (**f–j**) test. See also Supplementary Table 1.